Investigations on Dielectric, Transport, and Ferroelectric Properties of Ca-Modified $Bi_{0.80}La_{0.20}FeO_3$ Ceramic Synthesized by Solid State Reaction Route

Subhash Sharma[1,2] · Pawan Kumar[3] · Manish Kumar[4] · Vikash Singh[5] · Rosario I. Yocupicio-Gaxiola[6] · J. M. Siqueiros[1] · O. Raymond Herrera[1]

Abstract

Ca ion-modified $Bi_{0.80-x}Ca_xLa_{0.20}FeO_3$ (BCLFO) polycrystalline samples (with $x = 0.0$, 0.03, 0.06, and 0.12), synthesized by solid-state reaction, and their structural, dielectric, transport, and ferroelectric properties are explored. Rietveld analysis of XRD data revealed that Ca ions provoke structural distortions followed by a phase transition for $x = 0.12$. The Williamson–Hall analysis revealed that Ca doping enhances the distortion in FeO_6 octahedra, resulting in increases in strain and particle size. Scanning electron microscopy demonstrates a decrease in grain size with Ca doping. Room-temperature dielectric properties are remarkably enhanced with Ca incorporation when compared with those of undoped $Bi_{0.80}La_{0.20}FeO_3$ (BLFO). Furthermore, the ac conductivity of these samples has been investigated from room temperature to 500 °C and different conduction mechanisms were found in different temperature regions. Ca incorporation prevents Bi evaporation and fluctuation of Fe oxidation states, which is reflected in better ferroelectric polarization versus electric field (P–E) loops than those of BLFO ceramics. However, this behavior reverses for $x = 0.12$ due to a structural rhombohedral to orthorhombic phase transition.

✉ Subhash Sharma
subhash@ens.cnyn.unam.mx; subhi_77@rediffmail.com

1   Centro de Nanociencias y Nanotecnología, Universidad Nacional Autónoma de México, Km 107 Carretera Tijuana-Ensenada, A.P. 14, 22860 Ensenada, BC, México

2   CONACyT- Centro de Nanociencias y Nanotecnología, Universidad Nacional Autónoma de México, Km 107 Carretera Tijuana-Ensenada, A.P. 14, 22860 Ensenada, BC, México

3   School of Basic and Applied Sciences, K. R. Mangalam University, Gurugram, Haryana 122103, India

4   Department of Physics, Experimental Research Laboratory, ARSD College, University of Delhi, New Delhi 110021, India

5   ABES Engineering College, Ghaziabad, Uttar Pradesh 201009, India

6   Instituto Tecnologico Superior de Guasave, Carretera Internacional entronque a La Brechasn, Ejido Burroncito, SIN, Mexico

Introduction

Bismuth ferrate $BiFeO_3$ (BFO) is one of the widely studied multiferroic materials synthesized by researchers in both bulk and thin-film form.[1–4] Different routes have been used for the synthesis of BFO, such as solid-state reaction, single crystal growth, sol–gel, and other chemical routes. The dominant crystal phase of BFO at room temperature is rhombohedral belonging to the space group $R3c$.[2–4] In BFO, the $6s^2$ lone-pair electrons of Bi are responsible for its ferroelectricity, while its magnetic ordering is due to the partially filled d orbital of iron at the B site. The ferroelectric polarization of BFO has a reported magnitude of ~ 90 μC/cm^2 to 95 μC/cm^2 along the direction [111].[5,6] Its antiferromagnetic (G-type ordering) Neel temperature (~ 653 K) and ferroelectric Curie temperature (~ 1100 K) are well above room temperature.[7,8] Ferroelectric and magnetic properties, along with its photovoltaic response, make BFO a potential candidate for many applications in the field of electronics,

magnetism, spintronics, and photovoltaics, among others. Although BFO has advantageous room temperature multiferroic properties, it also has important drawbacks, such as high leakage current, low magnetoelectric coupling, poor ferroelectric ordering, weak ferromagnetic ordering at cryogenic temperatures, and difficult single-phase synthesis.[9–11] Ferroelectricity is particularly affected by the leakage current. Intensive research work is required to solve this problem before BFO becomes available for many applications. Recently, researchers have found that strategically doping BFO improves its physical properties.[12–18] Such improved properties of doped BFO have been associated with structural variabilities, and have been found to be extremely responsive to external stimuli, such as, e.g., magnetic/electric fields.[12,19] Along this line, several research groups have made efforts to dope BFO with lanthanide ions, calcium ions, and transition metal ions, such as Mn, Ti, and Cr.[20–25] It has been found that, when La doping in BFO is below 10%, it maintains the *R3c* symmetry; however, when it is 20% or beyond, its structure shifts to orthorhombic and/or tetragonal.[24] Likewise, it has been observed that La doping particularly improves the ferromagnetic ordering with a decrease in leakage current associated to the structural alteration. It is a familiar finding that the perovskite phase becomes more stable and improves its physical properties by incorporating dopants at the A and B sites.[26–28] It has also been reported that evaporation of Bi during the synthesis process and a reduction in oxygen vacancies is prevented by appropriately doping in BFO. In this paper, we report the effect of Ca doping on the structural, microstructural, and transport properties of $Bi_{0.80}La_{0.20}FeO_3$ (BLFO) ceramics.

Experimental

$Bi_{0.80-x}Ca_xLa_{0.20}FeO_3$ (BCLFO) with $0 \leq x \leq 0.12$ polycrystalline ceramic samples were prepared by solid-state reaction. The required amounts in a stoichiometric ratio were taken from high-purity reagents (> 99.98%) Bi_2O_3, Fe_2O_3, La_2O_3, and $CaCO_3$. The final powders were ground in an agate mortar for 4 h in acetone medium to produce a homogeneous mixture. After grinding, the powders were subjected to a heat treatment at 830°C for 2 h, ground again for 15 min and then pressed into 6-mm-diameter, 1-mm-thick disk pellets. The resulting ceramic pellet were sintered at 850°C for 2 h. For structural analysis, x-ray diffraction (XRD) patterns at room temperature were obtained with a Philips X-pert diffractometer with CuKα radiation. Microstructure studies were performed on cracked pellets using a JEOL-4500 scanning electron microscope (SEM). For electrical measurements, silver paste was used for the electrodes. The electrical measurements were performed using an HP 4284A LCR meter, and a Radiant Technologies Ferroelectric Tester was used for ferroelectric characterization.

Results and Discussion

Structural Properties

Phase formation for all the samples was determined by XRD measurements. Rietveld analysis was performed on the XRD data, revealing a rhombohedral (*R3c*) phase stable up to $x = 0.06$ and a phase transformation to orthorhombic phase for $x = 0.12$ (*Pbnm*). Figure 1a shows the experimental XRD patterns and corresponding Rietveld refinement profiles for $x = 0.06$ and 0.12; however, the full structural details were reported in a previous publication.[29] Figure 1b shows the unit cell for $x = 0.06$ as obtained with Vesta software. To calculate the microstrain and average particle size, the Williamson–Hall (W–H) approach was employed. The following equation between average crystallite size and microstrain has been used[30]:

$$\beta \cos \theta = \frac{k\lambda}{D} + 4\eta \sin \theta$$

where D is the average crystallite size, η is the microstrain, β denotes the total broadening of the peaks (the full width at half maximum) due to crystallite size and microstrain, k is the Scherrer's constant, and λ is the wavelength.[30] A graph of *4 sin θ* versus $\beta \cos \theta$ was plotted and is shown in Fig. 2. The average crystallite size and microstrain values were calculated using the intercept and slope of the plot, respectively, and are presented in Table I. The results of the W–H analysis demonstrate that Ca induces the lattice strain which increases with Ca concentration, as seen in Fig. 3. The average crystallite size is in the 36–66 nm range for these samples.

Dielectric Properties

Impedance measurements were carried out to study the temperature-dependent dielectric behavior of the samples. Figure 4 show the temperature-dependent dielectric constant (ε_r) and dielectric loss (tan δ), respectively, for typical frequencies (50 kHz, 100 kHz, and 1 MHz). The dielectric constant increases with increasing temperature, whereas it decreases with increasing frequency, indicating a normal dielectric behavior. It is interesting to observe a very small kink in the vicinity of 350°C at a frequency of 50 kHz, which disappears at 100 kHz and 1 MHz. Note that both ε_r above ~ 120°C and tan δ above ~ 200°C are frequency and temperature dependent.

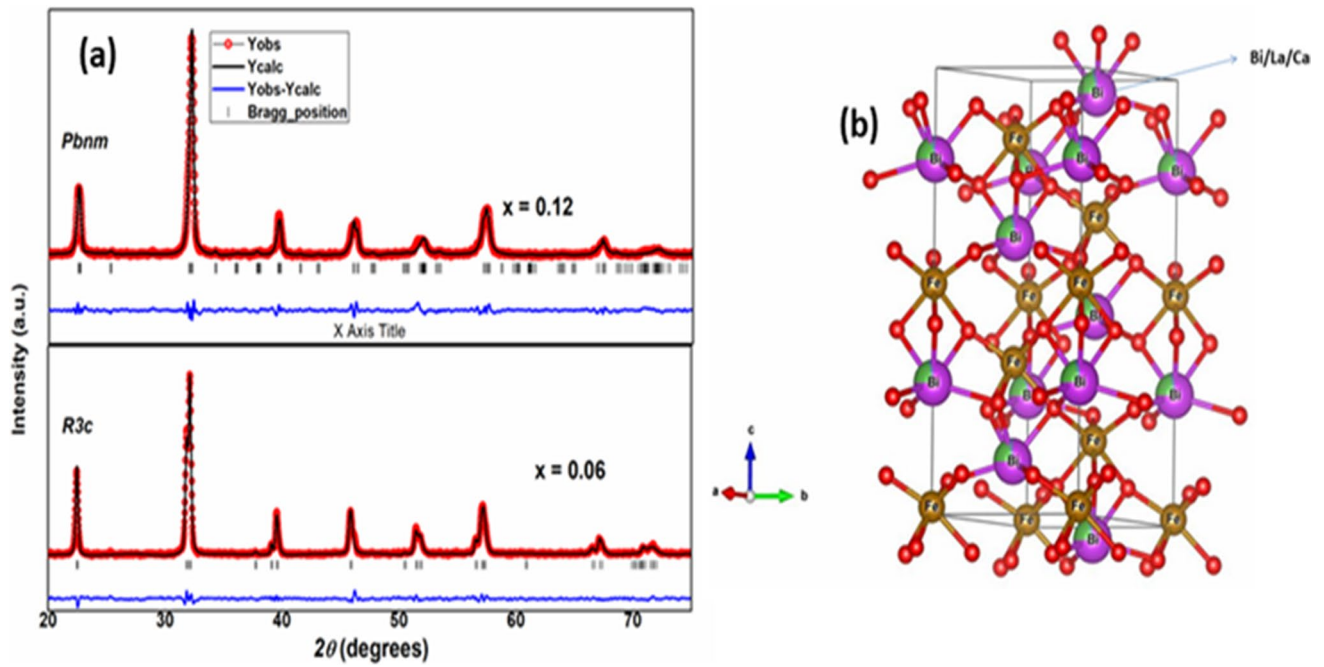**Fig. 1** (a) X-ray diffraction patterns with Rietveld refinement profiles of the $Bi_{0.80-x}Ca_xLa_{0.20}FeO_3$ for $x = 0.06$ and 0.12; (b) the unit cell of rhombohedral structure with $R3c$ symmetry for $x = 0.06$.

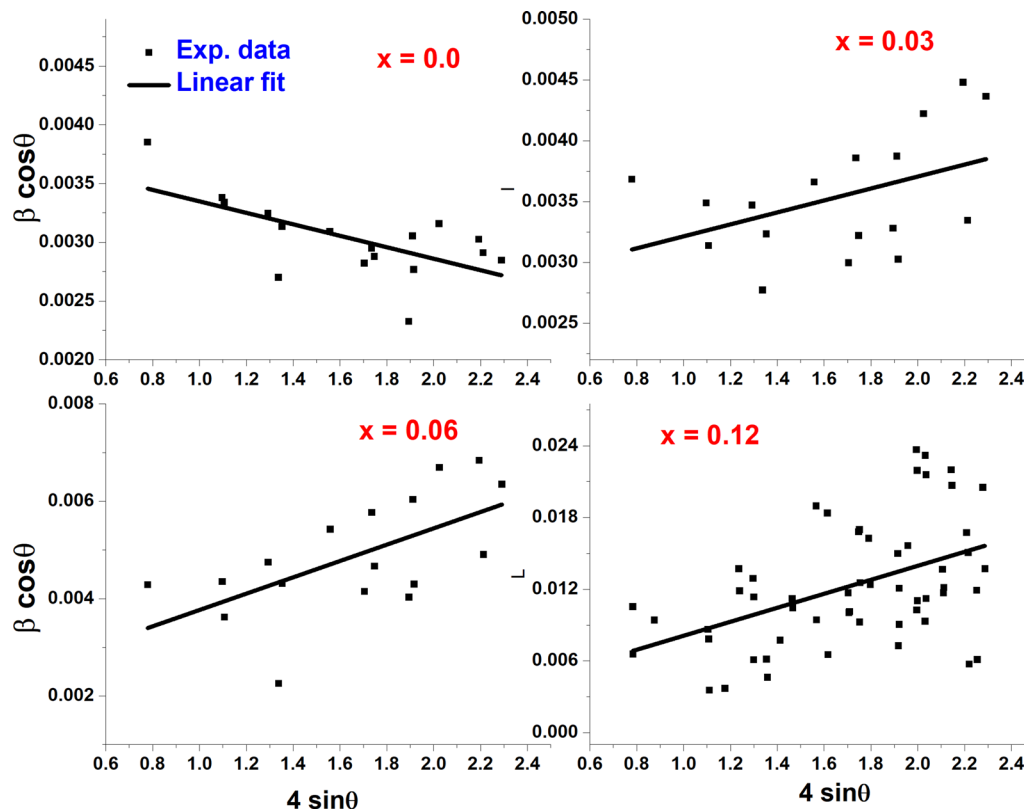**Fig. 2** Williamson–Hall plots of the $Bi_{0.80-x}Ca_xLa_{0.20}FeO_3$ samples ($0.0 \leq x \leq 0.12$).

Table I Dielectric parameters ε_r and tan δ and activation energy values obtained at different frequencies at room temperature for $Bi_{0.80-x}Ca_xLa_{0.20}FeO_3$ samples with $0.0 \leq x \leq 0.12$.

| x	Dielectric parameters		Activation energy (in eV)			
	ε_r	tan δ	I	II	III	IV
0.00	317	0.27	0.186	0.338	0.513	0.561
0.03	332	0.35	0.169	0.328	0.474	0.560
0.06	393	0.29	0.167	0.299	0.393	0.553
0.12	407	0.25	0.196	0.342	0.507	0.574

Such features in the dielectric plots are interesting and have been observed in other doped BFO materials. At a temperature around 150°C, the dielectric constant starts increasing for all the samples, which is related to the onset temperature in the dielectric loss (tan δ versus T plots) possibly due to the change of Fe^{3+} to Fe^{2+} ionic state.[31] In magneto-electrically ordered systems, the dielectric anomaly near the antiferromagnetic Néel (T_N) temperature is predicted by the Landau–Devonshire phase transition theory[2] as an effect of the disappearance of the magnetic order on the dielectric order. So, in the ε_r versus T plots, the ~ 350°C high temperature anomaly may be the result of a change in the magnetic order in BFO;[7] however, its disappearance for $x = 0.12$ may be due to another dominating dielectric mechanism. During sintering, Bi evaporation occurs mainly from the grain surfaces or interfaces and the grain boundaries. So, non-stoichiometry is an inherent problem in these Bi-deficient compounds. Oxygen vacancies are usually compensated by Bi vacancies, and therefore many oxygen vacancies in the interfacial region of grains and grain boundaries result in space charge accumulation, thus forming a barrier:

$$O_0 \rightarrow \left(\frac{1}{2}\right)O_2 \uparrow + V_0^{\bullet\bullet} + 2e' \tag{1}$$

$$V_O = V_O^{\bullet\bullet} + 2e' = \left(V_O^{\bullet\bullet} + e'\right) + e' \tag{2}$$

Thus, above a particular temperature, the presence of these free carriers results in an anomalous increase in tan δ. When compared, the tan δ values for the Ca-doped samples are found to be smaller. Figure 5 shows the Ca ion doping effect on the structure and the room-temperature dielectric properties. In Fig. 5, it is evident that the Ca ions enhance the insulating behavior for a higher Ca doping concentration by restricting Bi evaporation. The surface morphology of these samples in sintered pellets was measured using SEM. It can be observed (Fig. 6)
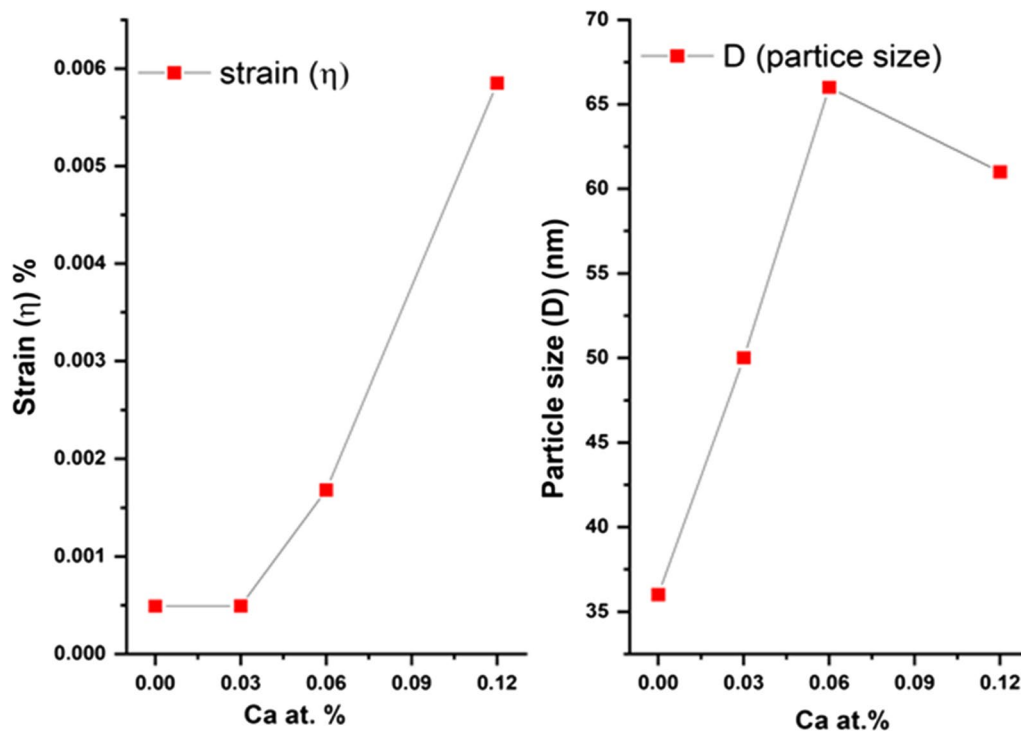
Fig. 3 The microstrain and particle size values obtained from W–H analysis of the $Bi_{0.80-x}Ca_xLa_{0.20}FeO_3$ system ($0.0 \leq x \leq 0.12$).
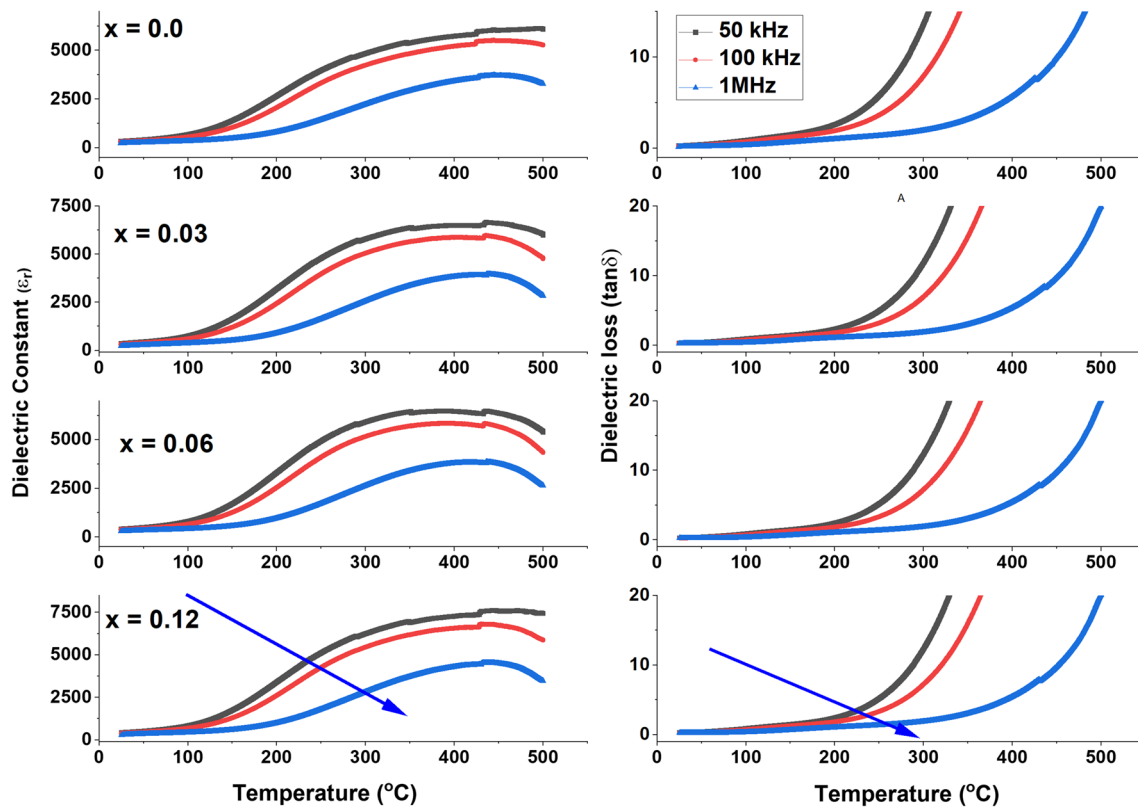
Fig. 4 Temperature-dependent dielectric response, ε_r and tan δ, for $Bi_{0.80-x}Ca_xLa_{0.20}FeO_3$ samples with $0.0 \leq x \leq 0.12$.
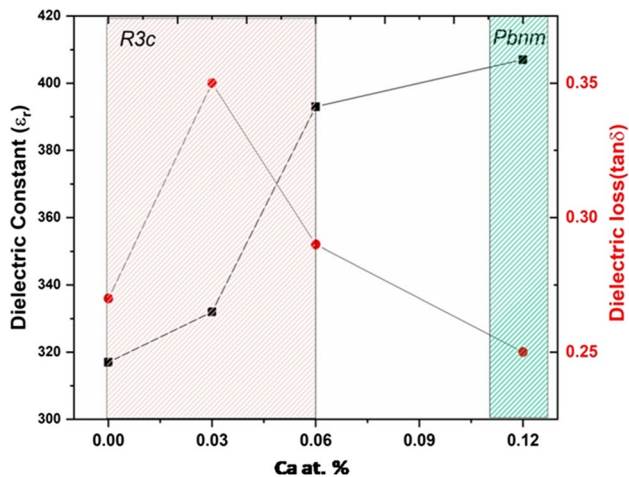
Fig. 5 Values of ε_r and tan δ at room temperature as functions of Ca at% for $Bi_{0.80-x}Ca_xLa_{0.20}FeO_3$ samples; the crystal symmetry is shown.

that the microstructure of the Ca-doped BLFO samples is dense with decreasing grain size as the doping concentration increases, indicating the crucial role of Ca doping in enhancing the density of the samples.

Transport Properties

Understanding the different kinds of conduction mechanisms in dielectric materials is very important for device fabrication with such materials. The different kinds of charge transport mechanisms are based on how the charge carriers react with the temperature and frequency (f). Moreover, conductivity is an intrinsic property of the material which depends on several factors like composition, structural symmetry, and the internal structure at atomic level. Therefore, to understand such behavior, the ac conductivity (σ_{ac}) of the samples calculated using the equation: $\sigma_{ac} = \varepsilon_r \cdot \varepsilon_0 \cdot \omega \cdot \tan \delta$, where ε_0 is the vacuum permittivity and ω is the angular frequency ($\omega = 2\pi f$). Figure 7 shows the $\ln(\sigma_{ac})$ versus 1000/T plots at some selected frequencies (50 kHz, 100 kHz, and 1000 kHz) for all the samples. It can be seen from these plots that a significant role is played by Ca^{2+} to alter the conduction behavior in the BLFO samples. For $x = 0.0$, the crossover between frequencies is present at higher temperature region. Moreover, frequency dependency has been observed at the lower temperatures (~ 30−230°C) for all the samples except for $x = 0.12$. Figure 8 shows the $\ln(\sigma_{ac})$ versus 1000/T plots at the 100 kHz frequency for all the compositions, reflecting the clear role of temperature in increasing the conductivity. Furthermore, to obtain information of the conduction
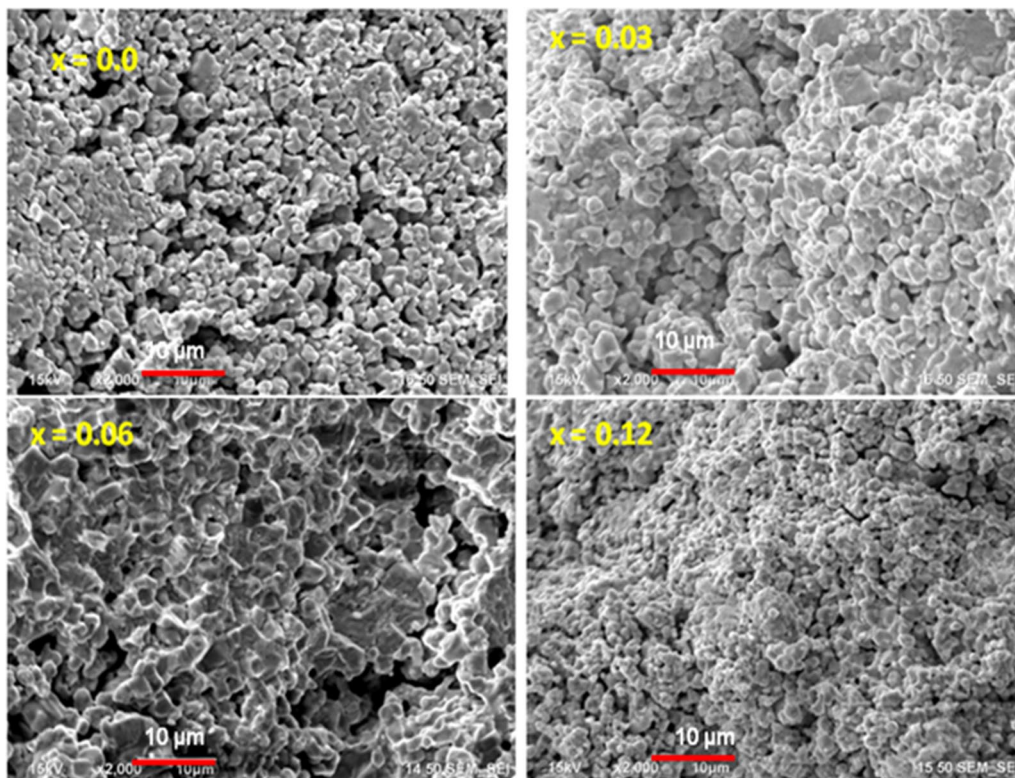
Fig. 6 Scanning electron micrographs of $Bi_{0.80-x}Ca_xLa_{0.20}FeO_3$ ceramic samples ($x = 0.00$, 0.03, 0.06, and 0.12).

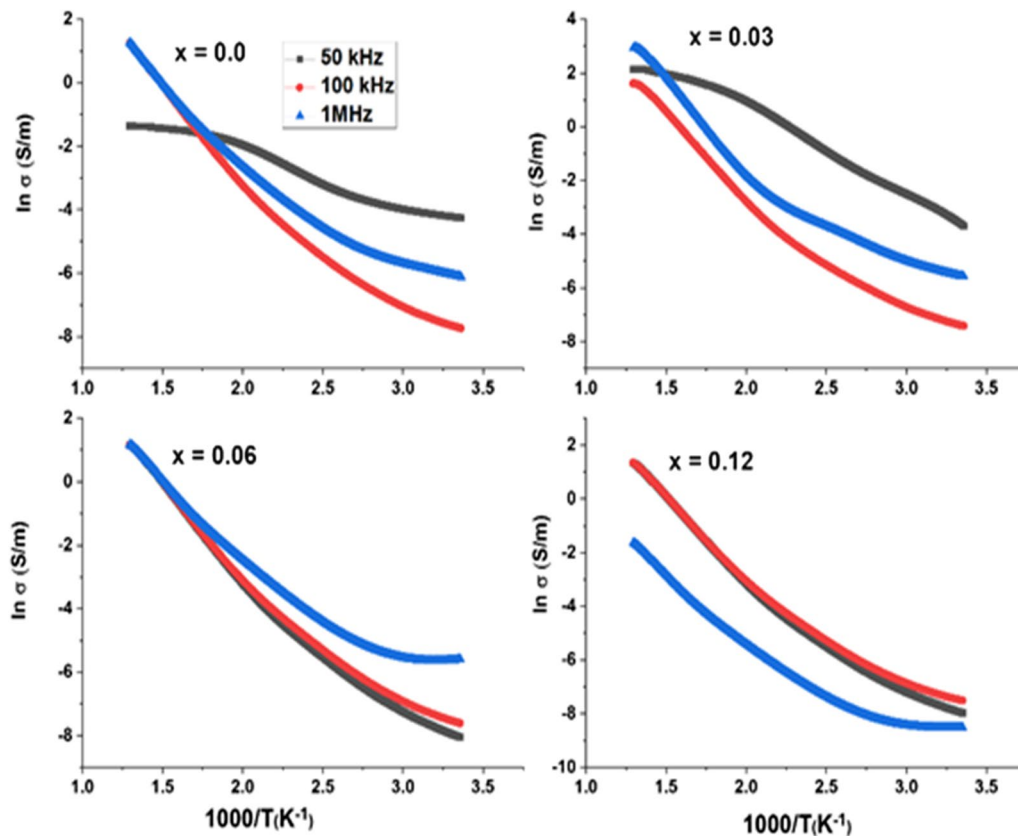**Fig. 7** Arrhenius plots (ln σ versus 1000/T) at different frequencies (50 kHz, 100 kHz, and 1 MHz) for $Bi_{0.80-x}Ca_xLa_{0.20}FeO_3$ samples with $0.0 \leq x \leq 0.12$.
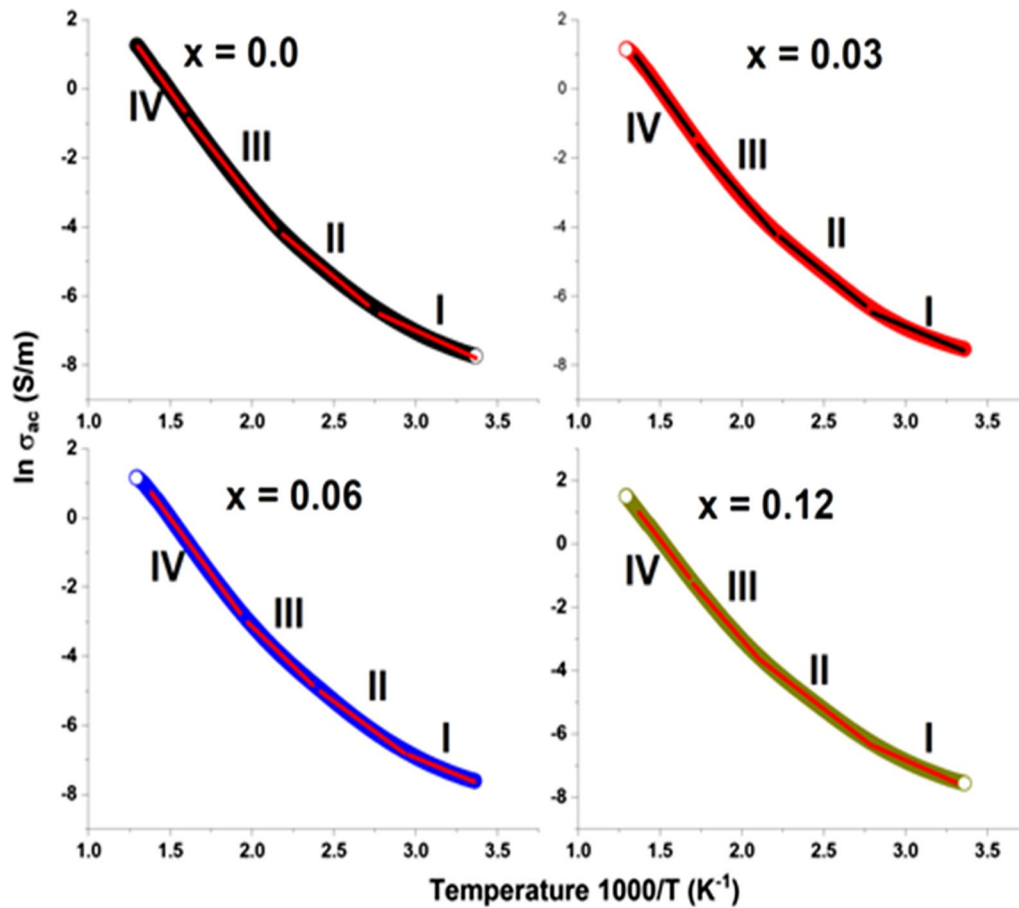
Fig. 8 Arrhenius plots (ln σ versus 1000/T) at 100 kHz for $Bi_{0.80-x}Ca_xLa_{0.20}FeO_3$ system with $0.0 \leq x \leq 0.12$.

mechanisms in different regions, the activation energy values were calculated using the Arrhenius equation:[32,33] $\sigma_{ac} = \sigma_0 exp(- E_A/kT)$, where k is Boltzmann's constant and E_A is the activation energy. In the present case, the ac conductivity at 100 kHz as a function of temperature was plotted and is shown in Fig. 8. To investigate in detail the conduction behavior of the sample, four different linear regions were identified in the curve. The values of the activation energies thus obtained are presented in Table I. As can be observed, small values of the activation energy are obtained at the lower temperature, whereas high activation energy values are at the higher temperatures, suggesting the presence of different conduction mechanisms in the samples. As observed in the 300–373 K temperature range (region I), the value of the activation energy is between 0.16 eV and 0.19 eV at 100 kHz (see Table I), suggesting a hopping charge mechanism of the electrons via oxygen vacancies. The increase in conductivity in the ~ 373–530 K temperature range (region II), where the activation energy values are between 0.29 eV and 0.34 eV, is ascribed to a small polaron hopping mechanism which is activated by the increase of the ferroelectric distortion with temperature.[34]

The III and IV temperature regions have activation energy values between 0.39 eV and 0.57 eV, where the conduction can be ascribed to the movement of single and doubly ionized oxygen vacancies, as reported for other perovskite materials.[32]

Ferroelectric Measurements

To analyze the ferroelectric nature of the samples, room-temperature hysteresis (P–E) loops were measured for all the compositions in the $Bi_{0.80-x}Ca_xLa_{0.20}FeO_3$ system at 50 Hz, and are shown in Fig. 9, from which it can be seen that the $x = 0.00$ (BLFO) sample exhibits better ferroelectric loops when compared with pure BFO, as described in our previously published report.[35] The substitution of Bi by Ca in the BLFO lattice improved the ferroelectric properties for compositions up to $x = 0.06$, and then declined for $x = 0.12$. The betterment of the ferroelectric parameters up to $x = 0.06$ can be understood in terms of the Ca ion improving the stereochemical activity of the A site, which is responsible for the ferroelectric properties of BFO. Furthermore, Ca doping controls the evaporation of Bi and the formation of oxygen vacancies, which further
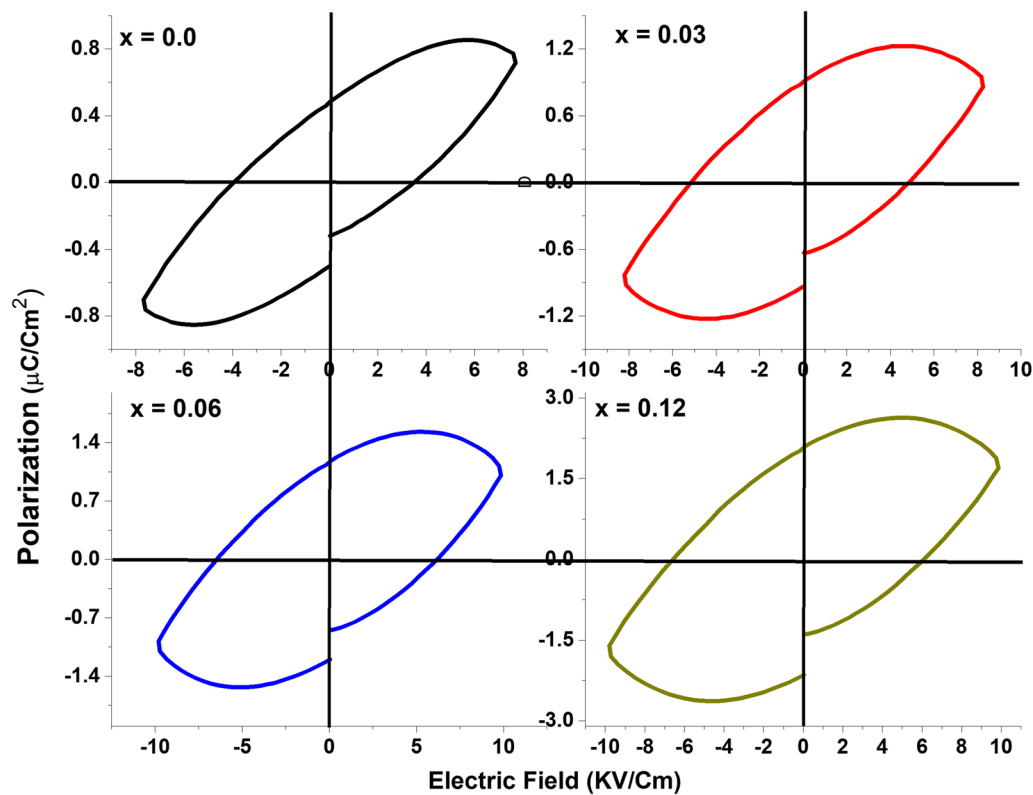
Fig. 9 P–E hysteresis loops for $Bi_{0.80-x}Ca_xLa_{0.20}FeO_3$ samples with $0.0 \leq x \leq 0.12$.

improves the insulating behavior of the samples. The decrease in the ferroelectric properties for $x = 0.12$ is attributed to the rhombohedral to orthorhombic phase transition, as verified by the structural analysis. In summary, an enhancement of the ferroelectric properties with Ca doping is observed even though no polarization saturation is achieved, and it is ascribed to the relatively stable domain formation, resulting in better ferroelectric characteristics for Ca-doped BLFO ceramics.

Conclusions

Polycrystalline Ca-doped BLFO ceramics samples were synthesized by solid-state reaction. No spurious impurity phases were detected in the XRD patterns. At higher concentrations ($x = 0.12$), the Ca incorporation induces a rhombohedral-to-orthorhombic structural phase transformation in the samples. The dielectric properties are improved by Ca doping because it inhibits evaporation of Bi during the sintering process, leading to a better dielectric behavior. A small kink around the Néel temperature in the dielectric plots confirms the magnetoelectric coupling in the samples. The temperature-dependent study of ac conductivity indicates a hopping charge mechanism in the ~ 300–373 K temperature range, followed by a preponderant small polaron

hopping mechanism in the ~ 373–530 K range, while, at higher temperatures, it is preponderantly ionized oxygen vacancy conduction. Ferroelectric properties improve with Ca ion doping up to $x = 0.06$, but decline for $x = 0.12$, due to the rhombohedral to the orthorhombic phase transition seen in the XRD analysis.

References

1. X. Chen, X. Li, H. Zhou, J. Sun, X. Li, and X. Yan, Phase evolution, microstructure, electric properties of $(Ba_{1-x}Bi_{0.67x}Na_{0.33x})(Ti_{1-x}Bi_{0.33x}Sn_{0.67x})O_3$ ceramics. *J. Adv. Ceram.* 8, 427 (2019).
2. S. Sharma, C.F. Sanchez, J.L. Sanchez Llamazares, J.M. Siqueiros, and O.R. Herrera, Unveiling quantum superparamagnetism by interacting monodomains in multiferroic Er-doped bismuth ferrate nanostructured particles. *J. Phys. Chem. C.* 125, 6449 (2021).
3. S. Sharma, M. Kumar, G. Srinet, J.M. Siqueiros, and O.R. Herrera, Structural, Raman analysis and exchange bias effects in

Mn doped multiferroic $Bi_{0.80}La_{0.10}Ca_{0.10}Fe_{1-x}Mn_xO_3$ ceramics. *Ceram. Int.* 47(5), 6834 (2021).

4. S.M. Selbach, T. Tybell, M. Einarsrud, and T. Grande, The ferroic phase transitions of $BiFeO_3$. *Adv. Mater.* 20, 3692 (2008).

5. G. Catalan, and J.F. Scott, Physics and applications of bismuth ferrite. *Adv. Mater.* 21(24), 2463 (2009).

6. Y.H. Chu, L.W. Martin, M.B. Holcomb, and R. Ramesh, Controlling magnetism with multiferroics. *Mater. Today* 10(10), 16 (2007).

7. J. Seidel, L.W. Martin, Q. He, Q. Zhan, Y.H. Chu, A. Rother, and R. Ramesh, Conduction at domain walls in oxide multiferroics. *Nat. Mater.* 8(3), 229 (2009).

8. S.V. Kiselev, Detection of magnetic order in ferroelectric $BiFeO_3$ by neutron diffraction. *Sov. Phys.* 7, 742 (1963).

9. N.A. Spaldin, S.W. Cheong, and R. Ramesh, Multiferroics: past, present, and future. *Phys. Today* 63(10), 38 (2010).

10. M.S. Bernardo, T. Jardiel, M. Peiteado, F.J. Mompean, M. Garcia-Hernandez, M.A. Garcia, and A.C. Caballero, Intrinsic compositional inhomogeneities in bulk Ti-doped $BiFeO_3$: microstructure development and multiferroic properties. *Chem. Mater.* 25(9), 1533 (2013).

11. T.J. Park, G.C. Papaefthymiou, A.J. Viescas, A.R. Moodenbaugh, and S.S. Wong, Size-dependent magnetic properties of single-crystalline multiferroic $BiFeO_3$ nanoparticles. *Nano Lett.* 7(3), 766 (2007).

12. D.V. Karpinsky, I.O. Troyanchuk, M.V. Bushinsky, S.A. Gavrilov, M.V. Silibin, and A. Franz, Crystal structure and magnetic properties of $Bi_{1-x}Ca_xFe_{1-x}Mn(Ti)_xO_3$ ceramics across the phase boundary. *J. Mater. Sci.* 51(23), 10506 (2016).

13. Y.J. Yoo, J.S. Hwang, Y.P. Lee, J.S. Park, J.Y. Rhee, J.H. Kang, and M.S. Seo, Origin of enhanced multiferroic properties in Dy and Co co-doped $BiFeO_3$ ceramics. *J. Magn. Magn. Mater.* 374, 669 (2015).

14. A. Singh, V. Pandey, R.K. Kotnala, and D. Pandey, Direct evidence for multiferroic magnetoelectric coupling in $0.9BiFeO_3$–$0.1BaTiO_3$. *Phys. Rev. Lett.* 101(24), 247602 (2008).

15. C.H. Yang, D. Kan, I. Takeuchi, V. Nagarajan, and J. Seidel, Doping $BiFeO_3$: approaches and enhanced functionality. *Phys. Chem. Chem. Phys.* 14(46), 15953 (2012).

16. M. Kumar, S. Shankar, R.K. Kotnala, and O. Parkash, Evidences of magneto-electric coupling in BFO–BT solid solutions. *J. Alloys Compd.* 577, 222 (2013).

17. L. Yao, X. Wu, S. Yang, and Y. Zhang, Structural and optical properties of Ca doped $BiFeO_3$ thin films prepared by a sol–gel method. *Ceram. Int.* 43, S470–S473 (2017).

18. H. Deng, M. Zhang, Z. Hu, Q. Xie, Q. Zhong, J. Wei, and H. Yan, Enhanced dielectric and ferroelectric properties of Ba and Ti co-doped $BiFeO_3$ multiferroic ceramics. *J. Alloys Compd.* 582, 273 (2014).

19. D. Kan, L. Pálová, V. Anbusathaiah, C.J. Cheng, S. Fujino, V. Nagarajan, and I. Takeuchi, Universal behavior and electric-field-induced structural transition in rare-earth-substituted $BiFeO_3$. *Adv. Funct. Mater.* 20(7), 1108 (2010).

20. X. Wang, S.Y. Wang, W.F. Liu, X.J. Xi, H. Zhang, F. Guo, and J.B. Yang, Novel electrical conductivity properties in Ca-doped $BiFeO_3$ nanoparticles. *J. Nanopart. Res.* 17(5), 1 (2015).

21. Y. Tian, F. Xue, Q. Fu, L. Zhou, C. Wang, H. Gou, and M. Zhang, Structural and physical properties of Ti-doped $BiFeO_3$ nanoceramics. *Ceram. Int.* 44(4), 4287–4291 (2018).

22. S.T. Zhang, Y. Zhang, M.H. Lu, C.F. Du, Y.F. Chen, Z.G. Liu, and X.Q. Pan, Substitution-induced phase transition and enhanced multiferroic properties of $Bi_{1-x}La_xFeO_3$ ceramics. *Appl. Phys. Lett.* 88(16), 162901 (2006).

23. B. Wang, X. Tian, X. Song, L. Ma, S. Yu, C. Hao, and Q. Lei, Smart electrorheological behavior of Cr-doped multiferroelectric $FeBiO_3$. *Colloid. Surf. A.* 461, 184 (2014).

24. Q. Zhang, X. Zhu, Y. Xu, H. Gao, Y. Xiao, D. Liang, and D. Xiao, Effect of La^{3+} substitution on the phase transitions, microstructure and electrical properties of $Bi_{1-x}La_xFeO_3$ ceramics. *J. Alloys Compd.* 546, 57 (2013).

25. L.H. Yin, W.H. Song, X.L. Jiao, W.B. Wu, X.B. Zhu, Z.R. Yang, and Y.P. Sun, Multiferroic and magnetoelectric properties of $Bi_{1-x}Ba_xFe_{1-x}Mn_xO_3$ system. *J. Phys. D Appl. Phys.* 42(20), 205402 (2009).

26. P.M. Razad, K. SaravanKumar, V.R. Reddy, R.J. Choudhary, K. Jeyadheepan, and K. Mahalakshmi, Tailoring the size and magnetization of titanium-doped $BiFeO_3$ Nanorods. *J. Electron. Mater.* 50, 1075 (2021).

27. D.V. Thang, V.Q. Nguyen, N.M. Hung, L.T.M. Anh, N.C. Khang, B.D. Tu, D.T. Xuan Thao, and N.V. Minh, Structural, optical, ferroelectric and ferromagnetic properties of $Bi_{1-x}Gd_xFeO_3$ materials. *J. Electron. Mater.* 49, 4443–4449 (2020).

28. P. Kumar, N. Shankhwar, A. Srinivasan, and M. Kar, Oxygen octahedra distortion induced structural and magnetic phase transitions in $Bi_{1-x}Ca_xFe_{1-x}Mn_xO_3$ ceramics. *J. Appl. Phys.* 117(19), 194103 (2015).

29. S. Sharma, M. Kumar, J.M. Siqueiros, and O.R. Herrera, Phase evolution, magnetic study and evidence of spin-two phonon coupling in Ca modified $Bi_{0.80}La_{0.20}FeO_3$ ceramics. *J. Alloys Compd.* 827, 154223 (2020).

30. V. Biju, N. Sugathan, V. Vrinda, and L. Salin, Estimation of lattice strain in nanocrystalline silver from x-ray diffraction line broadening. *J. Mater. Sci.* 43, 1175–1179 (2008).

31. S. Sharma, V. Singh, and R.K. Dwivedi, Electrical properties of $(1-x)BFO–(x)$ PZT multiferroics synthesized by sol–gel method: transition from relaxor to non-relaxor. *J. Alloys Compd.* 682, 723 (2016).

32. L.E. Cross, Relaxor ferroelectrics. *Ferroelectrics* 76, 241–267 (1987).

33. R.K. Dwivedi, D. Kumar, and O. Parkash, Valence compensated perovskite oxides system $Ca_{1-x}La_xTi_{1-x}Cr_xO_3$: part-II electrical transport behaviour. *J. Mater. Sci.* 36, 3649–3655 (2001).

34. O. Raymond, R. Font, N. Suárez, J. Portelles, and J.M. Siqueiros, Frequency-temperature response of ferroelectromagnetic $Pb(Fe_{0.5}Nb_{0.5})O_3$ ceramics obtained by different precursors. Part I. Structural and thermo-electrical characterization. *J. Appl. Phys.* 97, 084107 (2005).

35. S. Sharma, V. Singh, R.K. Dwivedi, R. Ranjan, A. Anshul, S.S. Amritphale, and N. Chandra, Phase transformation, improved ferroelectric and magnetic properties of $(1-x)BiFeO_3$–$Pb(Zr_{0.52}Ti_{0.48})O_3$ solid solutions. *J. Appl. Phys.* 115(22), 224106 (2014).